Available online at www.sciencedirect.com
ScienceDirect
Journal of the European Ceramic Society 29 (2009) 2087–2095
www.elsevier.com/locate/jeurceramsoc

Spark plasma sintering and pressureless sintering of SiC using aluminum borocarbide additives

Sea-Hoon Lee [a,*], Hidehiko Tanaka [a], Yutaka Kagawa [b]

[a] National Institute for Materials Science, 1-1 Namiki, Tsukuba, Ibaraki 305-0044, Japan
[b] Research Center for Advanced Science and Technology (RCAST), The University of Tokyo, 4-6-1 Komaba, Meguro-Ku, Tokyo 153-8505, Japan

Received 2 July 2008; received in revised form 23 November 2008; accepted 3 December 2008
Available online 13 January 2009

Abstract

Aluminum borocarbide powders (Al_3BC_3 and $Al_8B_4C_7$) were synthesized, and the ternary powders were used as a sintering additive of SiC. The densification of SiC was nearly completed at 1670 °C using spark plasma sintering (SPS) and pressureless sintering was possible at 1950 °C. The sintering behavior of SiC using the new additive systems was nearly identical with that using the conventional Al–B–C system, but grain growth was suppressed when adding the borocarbides. In addition, oxidation of the fine additive powders did not intensively occur in air, which has been a problem in the case of the Al–B–C system for industrial application. The hardness, Young's modulus and fracture toughness of a sintered SiC specimen were 21.6 GPa, 439 GPa and 4.6 MPa $m^{1/2}$, respectively. The ternary borocarbide powders are efficient sintering additives of SiC.

Keywords: Calcination; Sintering; Mechanical properties; SiC; Structural applications

1. Introduction

A mixture of aluminum, boron (or B_4C) and carbon (here after termed Al–B–C) has been recently intensively investigated as a sintering additive of SiC because it reduces the sintering temperature and improves the fracture toughness of SiC.[1,2] In spite of the advantages, large flakes of metal aluminum may form during milling process, which may cause the formation of flaws and the inhomogeneous distribution of additives in sintered SiC. The flakes can be crushed by increasing milling energy, but the resultant powder mixture may require careful handling in an inert atmosphere due to the rapid oxidation reaction of the crushed fine aluminum powder in air.[3] In addition, Moberlychan et al. reported that when the size of aluminium particles were larger than 3 μm, residual secondary phases were commonly formed with only a limited amount of the additives actually incorporated as the grain boundary interlayer.[4]

After the first report of Inoue et al. about $Al_8B_4C_7$ at 1980, the presence or formation of the phase has been observed until recently.[5–9] At 1996, Hillebrecht and Meyer analyzed the structure of the ternary compound and reported that the correct formula of the compound is Al_3BC_3.[10–12] The present authors also recently experimentally proved that Al_3BC_3 is the correct phase by identifying the presence of a secondary phase in a sintered $Al_8B_4C_7$ while sintered Al_3BC_3 was mono-phase.[13]

Researches about the sintering behavior and mechanical properties of SiC using the Al–B–C additive system have been reported.[1,5] However, application of the aluminium borocarbides as sintering additives of SiC has never been reported. Compared to the conventional Al–B–C system, the ternary compounds are expected to be mixed more homogeneously with SiC and the total process may become simple and safe because the borocarbide powders having sub-micrometer in size may not intensively react with air.

Here we report the application of Al_3BC_3, instead of the conventional Al–B–C powder mixture, as a sintering additive of SiC. A ternary powder having composition of $Al_8B_4C_7$ was also synthesized and tested (here after termed $Al_8B_4C_7$). The densification behavior of the SiC containing the additives during spark plasma sintering (SPS) or pressureless sintering was investigated and the microstructure and mechanical properties of the sintered SiC were analyzed.

* Corresponding author. Tel.: +82 55 280 3344; fax: +82 55 280 3392.
E-mail address: seahoon1@kims.re.kr (S.-H. Lee).

0955-2219/$ – see front matter © 2008 Elsevier Ltd. All rights reserved.
doi:10.1016/j.jeurceramsoc.2008.12.006

Table 1
Theoretical chemical composition of the systems for the preparation of the ternary compounds or the Al–B–C powder mixtures (wt%).

Abbreviation	Al	B_4C	C
3Al–B–3C, Al_3BC_3	63.3	10.8	25.9
8Al–4B–7C, $Al_8B_4C_7$	62.9	16.1	21.0

2. Experimental procedure

Aluminum (Reagent grade, Koso Chemical Inc., Tokyo, Japan), B_4C (Grade HD20, H.C. Starck, Goslar, Germany), and carbon (carbon black, MA-600B, Mitsubishi Chem., Tokyo, Japan) were used as the starting powders. The raw powders (3Al:B:3C or 8Al:4B:7C by molar ratio, termed 3Al–B–3C or 8Al–4B–7C, Table 1) were mixed in ethanol for 10 min using an ultrasonifier (US-1200T, Nissei, Tokyo, Japan), and the mixed slurries were dried with stirring using a hot plate. Then, the powder mixtures were calcined at 1800 °C for 2 h in high purity Ar (purity of Ar: >99.998%, heating rate: 75 °C/min up to 1500 °C, 30 °C/min above 1500 °C) using a induction furnace (FVHP-1-3, Fuji Dempa Kogyo Corp., Tokyo, Japan). During the calcination, the powder mixtures were placed in a graphite mold and were tightly capped using a BN slurry in order to minimize the vaporization of aluminum during calcination. The average particle size (equivalent spherical diameter) of the synthesized compound before and after an attrition milling was measured using a laser particle size analyzer (1064, CILAS, Orleans, France). Aluminum, boron and carbon content in the synthesized Al_3BC_3 was measured using an inductively coupled plasma atomic emission spectrometry (analyzed components: aluminium and boron, ICP-AES, Optima 3300DV, PerkinElmer, Wellesley, MA) and infrared absorption method (analyzed component: carbon, CS 444-LS, Leco, St. Joseph, MI), respectively.

Al_3BC_3, the $Al_8B_4C_7$ or the Al–B–C powder was mixed with α-SiC (UF-15, polytype: mainly 6H-SiC, H.C. Starck, Goslar, Germany) using a planetary mill with SiC ball, SiC jar and ethyl-alcohol at 250 revolutions/min (r.p.m.) for 24 h. Then, the slurries were dried with stirring using a hot plate, and the obtained powder mixtures were sieved and densified using SPS (Dr. Sinter SCM 3000, Sumitomo Coal Mining Co. Ltd., Japan, heating within 3 min from 600 °C to 1900 °C) at 1900 °C for 3 min under 40 MPa pressure in vacuum. During heating using SPS apparatus, the temperature at the surface of the graphite die was reported to be lower than that of the specimen due to the radiation cooling.[14] Consequently, a hole which directly reached to the sample surface was punched at the middle of the carbon mold (diameter: 1.5 mm) in order to directly measure the temperature of the sample surface using a pyrometer. In addition, the carbon mold was insulated by a carbon felt in order to minimize the radiation cooling.[14]

SiO_2 is generally formed at the surface of SiC powder by the reaction with humidity.[15] The oxide forms liquid phase during heating, which may promote densification of SiC at the expense of high temperature properties due to the low melting temperature of the grain boundary phase.[16] Consequently, parts of the powder mixture were heated at 1500 °C in vacuum for 10 min to remove SiO_2 before sintering at 1900 °C. The oxygen content of a powder mixture composed of SiC and 10 wt% Al_3BC_3 (termed SiC–10Al_3BC_3) was measured after the heating at 1500 °C in vacuum for 30 min using an inert gas carrying melting-infrared absorptiometer (TC-600, Leco, St. Joseph, MI).

The SiC–10Al_3BC_3 powder and a powder mixture composed of SiC and 7.5 wt% Al_3BC_3 (termed SiC–7.5Al_3BC_3) were compacted to pellets (diameter: 1.3 cm, thickness: 0.7 cm) under 293 MPa pressure using a cold isostatic press (CIP), and were sintered at 1950–2050 °C for 2 h in 0.1 MPa Ar (heating rate: 75 °C/min up to 1500 °C, 30 °C/min above 1500 °C).

After sintering, the density of the specimens was analyzed using Archimedes' method at room temperature. The effects of sintering temperature on the microstructure and phase formation of the samples were analyzed by scanning electron microscopy (SEM, JSM-6700F, JEOL, Tokyo, Japan) and X-ray powder diffraction (XRD, JDX-3500, JEOL, Tokyo, Japan) with Cu Kα radiation. The spatial diameter of the SiC grains was estimated based on the ASTM standard.[17] Young's modulus was measured using an ultrasonic tester at 20–22 °C (5072PR, Panametrics, Boston, MA), and hardness and fracture toughness of the samples were obtained using a Vickers indenter (AVK-A, Akashi, Tokyo, Japan; loading condition: 10 kg, 15 s) according to Japanese Industrial Standard using the following formulae[18,19]:

$$\mathrm{HV} = 18.54\frac{P}{d^2} \tag{1}$$

$$K_C = 0.026\frac{E^{1/2}P^{1/2}(d/2)}{(C/2)^{3/2}} \tag{2}$$

where HV: Vickers hardness (GPa), P: applied force for indentation (N), d: average diagonal length of indent (m), K_C: fracture toughness (Pa m$^{1/2}$), E: Young's modulus (Pa), and C: average crack length (m).

The chemical distribution of the constituent materials in the SiC grains of a pressureless sintered SiC–10Al_3BC_3 sample was measured using an energy dispersive spectroscopy (EDS, Phoenix, EDAX, Mahwah, NJ) and electron probe microanalyzer (EPMA, JXA8900RL, JEOL). High resolution transmission electron microscopy (HRTEM, JEM-4000EX,

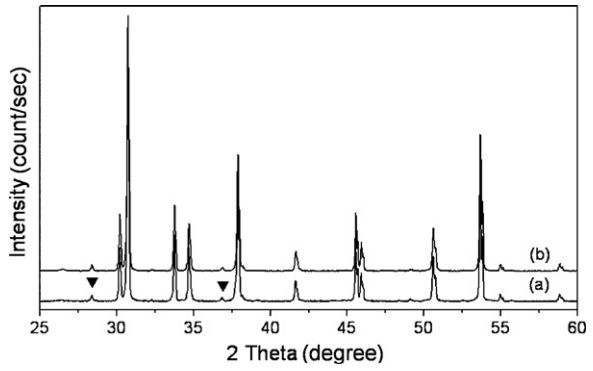

Fig. 1. XRD data of calcined powders having the composition of (a) $Al_8B_4C_7$ and (b) Al_3BC_3 (▼: unidentified peaks; others: $Al_8B_4C_7$ peaks reported by Inoue et al.[6]).

Table 2
Chemical composition of the synthesized Al_3BC_3 before and after heat treatment at 1500 °C for 30 min in vacuum.

	Al		B		C	
	Before	After	Before	After	Before	After
Composition (wt%)	62.4	56.7	8.4	9.9	27.7	30.3

JEOL) was performed to examine the nature of the grain boundary.

3. Results and discussion

3.1. Properties of aluminium borocarbide powders

Table 1 shows the chemical composition of Al_3BC_3 and the $Al_8B_4C_7$. Al content in the synthesized ternary powders decreased slightly compared to the stoichiometric values (Tables 1 and 2) due to vaporization at high temperature. The partial pressure of molten aluminum (melting point: 660 °C) was reported to be 2.28×10^3 Pa at 1727 °C in 0.1 MPa Ar.[20] The reduction of boron or carbon content did not occur after calcination because the vapor pressure of boron and carbon is much lower than that of aluminum. The melting temperature of both the components is higher than 2000 °C.[21]

Fig. 1 shows the XRD data of Al_3BC_3 and the $Al_8B_4C_7$. In spite of the difference of chemical composition, the peaks of both the powders were nearly identical. Shift of peaks, which indicates the formation of solid solution, did not distinctly occur in the $Al_8B_4C_7$. The results indicate that the excess components in the $Al_8B_4C_7$ presumably formed an amorphous secondary phase. The peaks of the synthesized powders were very similar to the data which were obtained from a single crystal.[6]

Table 2 exhibits the decrease of aluminum content and consequent formation of excess boron and carbon after the heating of Al_3BC_3 at 1500 °C in vacuum. Clearly, aluminum in the ternary compound vaporized at 1500 °C in vacuum. The oxygen content of the SiC–10Al_3BC_3 powder was 2.6 wt% after heating at 1400 °C for 10 min in vacuum, which value decreased to 1.5 wt% at 1500 °C due to the decomposition of SiO_2 by carbothermal reduction.[22] Carbon, which is required for removing SiO_2, was mainly supplied from the decomposed Al_3BC_3. In addition, the UF-15 SiC powder contained small amount of residual free carbon (0.2 wt%).

Fig. 2 displays the morphology of the additive powder before and after planetary milling for 24 h. Large aluminium flakes were observed in the Al–B–C system. The size of some flakes was larger than 100 μm (Fig. 2(a)). The as-fabricated Al_3BC_3 powder had irregular shape. The average particle size of the powder was 14.1 μm (Fig. 2(b)). However, the compound powder could be pulverized into sub-micrometer in size (Fig. 2(c)) and the fine powder did not suffer from rapid oxidation in air. The SiC + Al_3BC_3 mixture did not contain large Al_3BC_3 particles. EDS analysis informed that the rather large particles shown in Fig. 2(d) were SiC. The results indicated that the

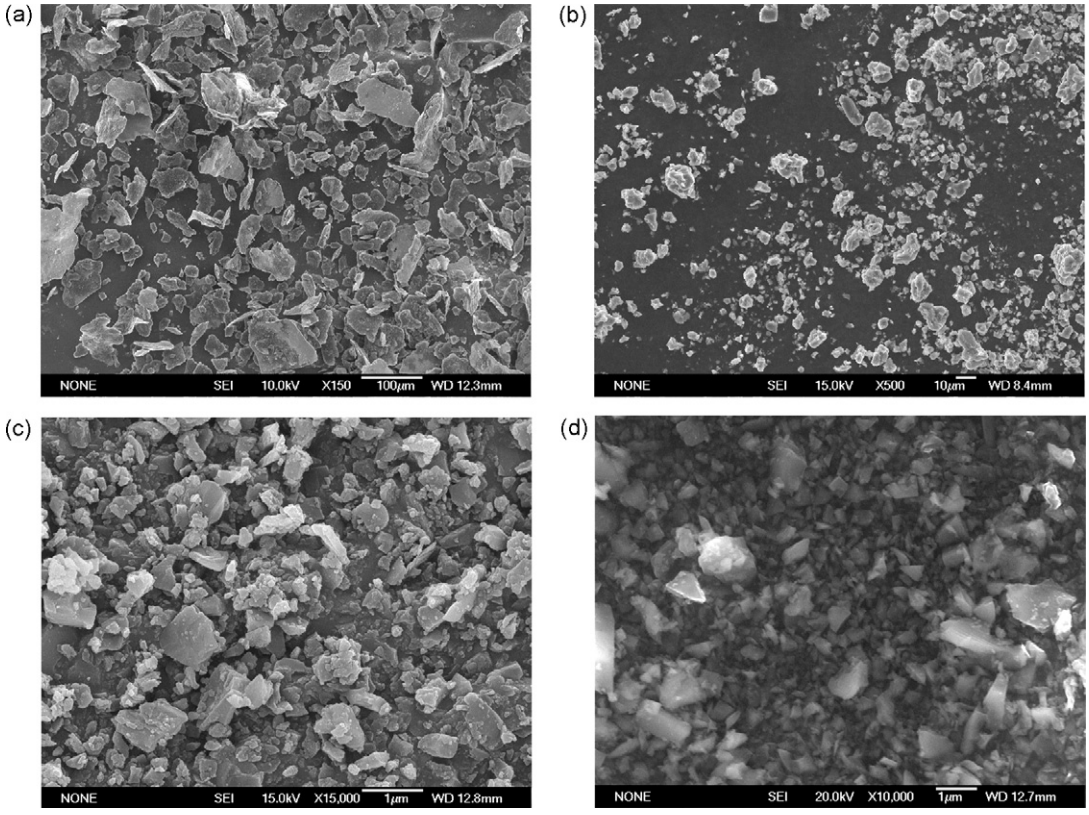

Fig. 2. Morphology of powders before and after planetary milling. (a) Al–B–C (150×), (b) Al_3BC_3, before milling (500×), (c) Al_3BC_3, 250 r.p.m., 24 h (15,000×), (d) SiC + 10 wt% Al_3BC_3, 210 r.p.m., 24 h (10,000×).

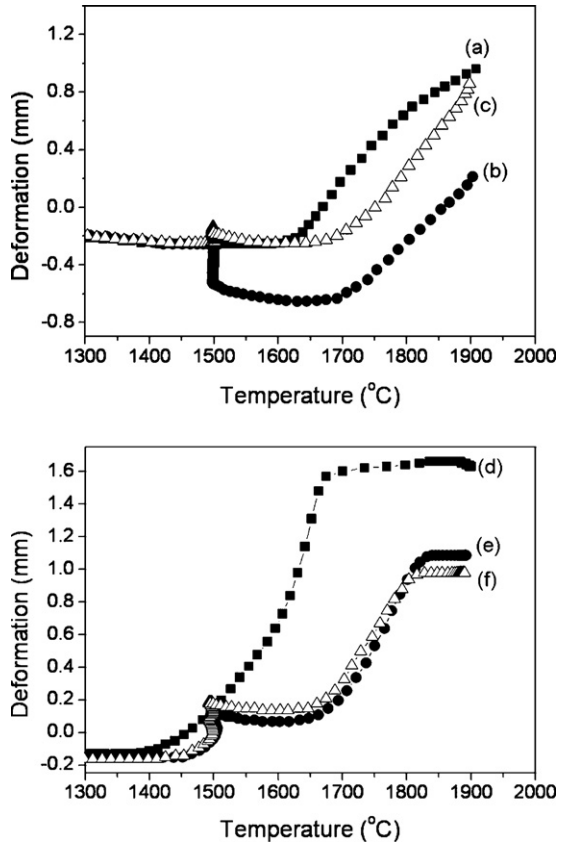

Fig. 3. Shrinkage of SiC with 10 wt% additives during sintering. Abbreviations for the heating conditions are described in Table 3. (a) Al_3BC_3, SPS, (b) Al_3BC_3, SPS anneal, (c) 3Al–B–3C, SPS anneal, (d) $Al_8B_4C_7$, SPS, (e) $Al_8B_4C_7$, SPS anneal and (f) 8Al–4B–7C, SPS anneal.

ternary compound powder was crushed into sub-micrometer in size during milling, and was rather homogeneously mixed with SiC.

3.2. Densification and microstructure

Fig. 3(a)–(c) visualizes the shrinkage of the SiC–10Al_3BC_3 or SiC containing 10 wt% 3Al–B–3C (termed SiC–3Al–B–3C) during SPS under 40 MPa pressure. The onset temperatures were more precisely analyzed using the differentiation of the deformation curves (data not shown). The onset temperature of shrinkage of the SiC–10Al_3BC_3 was 1589 °C (Fig. 3(a)), which increased to 1677 °C after heating at 1500 °C for 10 min in vacuum (Fig. 3(b)). The decrease of surface area during heating at 1500 °C and the reduction of the driving force for densification are believed to be the main reason for the increase of the sintering temperature.[23] The decomposition of SiO_2 during heating at 1500 °C and consequent depletion of a liquid phase is considered as another possible reason. TEM observation informed the absence of an amorphous layer in between SiC grains (Fig. 4).

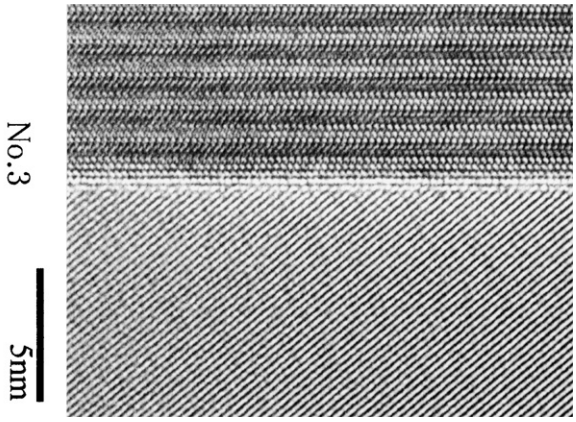

Fig. 4. High resolution TEM image showing the nature of the grain boundary in the SiC containing 10 wt% $Al_8B_4C_7$.

The onset temperature of sintering shrinkage (1677–1682 °C) and density after sintering (3.13–3.15 g/cm^3) were not strongly affected by the type of additives (3Al–B–3C or Al_3BC_3, Table 3). In both cases, densification was nearly completed within 1–2 min at 1900 °C. However, the grain size of the SiC–3Al–B–3C is clearly larger than that of the SiC–10Al_3BC_3 (Fig. 5(a) and (b)), indicating that the grain growth of SiC was more intensive when using the Al–B–C.

SiC containing 10 wt% $Al_8B_4C_7$ (termed SiC–$Al_8B_4C_7$) began to shrink at 1343 °C and sintering shrinkage was nearly finished at 1680 °C (Fig. 3(d)). After the heating of the

Table 3
Relative density and some mechanical properties of the sintered SiC. Sintering condition: SPS—heating up to 1900 °C within 3 min in vacuum under 40 MPa. Holding at 1900 °C for 3 min. SPS anneal—heating up to 1500 °C within 2 min in vacuum under 40 MPa, holding at 1500 °C for 10 min and heating again up to 1900 °C within 1 min. Holding at 1900 °C for 3 min. Pressureless—pressureless sintering in Ar for 2 h (heating rate: 75 °C/min up to 1500 °C, 30 °C/min above 1500 °C).

Condition	Density (g/cm^3)	Young's modulus (GPa)	Hardness (GPa)	Fracture toughness (MPa m$^{1/2}$)
SiC–3Al_3BC_3, SPS anneal	3.13	415	25.4 ± 1.0	3.2 ± 0.2
SiC–5Al_3BC_3, SPS anneal	3.17	409	26.4 ± 1.2	3.3 ± 0.1
SiC–7.5Al_3BC_3, SPS anneal	3.16	399	23.6 ± 1.0	3.6 ± 0.3
SiC–10Al_3BC_3, SPS anneal	3.15	390	24.8 ± 2.2	4.5 ± 0.3
SiC–10Al_3BC_3, SPS	3.11	376	20.6 ± 0.8	4.5 ± 0.3
SiC–3Al–B–3C, SPS anneal	3.13	383	22.8 ± 0.5	4.0 ± 0.2
SiC–3Al–B–3C, SPS	3.12	382	23.3 ± 0.5	3.6 ± 0.2
SiC–7.5Al_3BC_3, pressureless, 1950 °C	2.95	360	21.3 ± 1.6	3.6 ± 0.3
SiC–7.5Al_3BC_3, pressurelss, 2000 °C	2.99	379	22.0 ± 1.4	4.0 ± 0.1
SiC–7.5Al_3BC_3, pressurelss, 2050 °C	2.87	340	18.5 ± 0.9	4.1 ± 0.2
SiC–$Al_8B_4C_7$, SPS anneal	3.11	439	21.6 ± 0.9	4.6 ± 0.2
SiC–$Al_8B_4C_7$, SPS	3.10	384	21.7 ± 1.2	4.4 ± 0.3

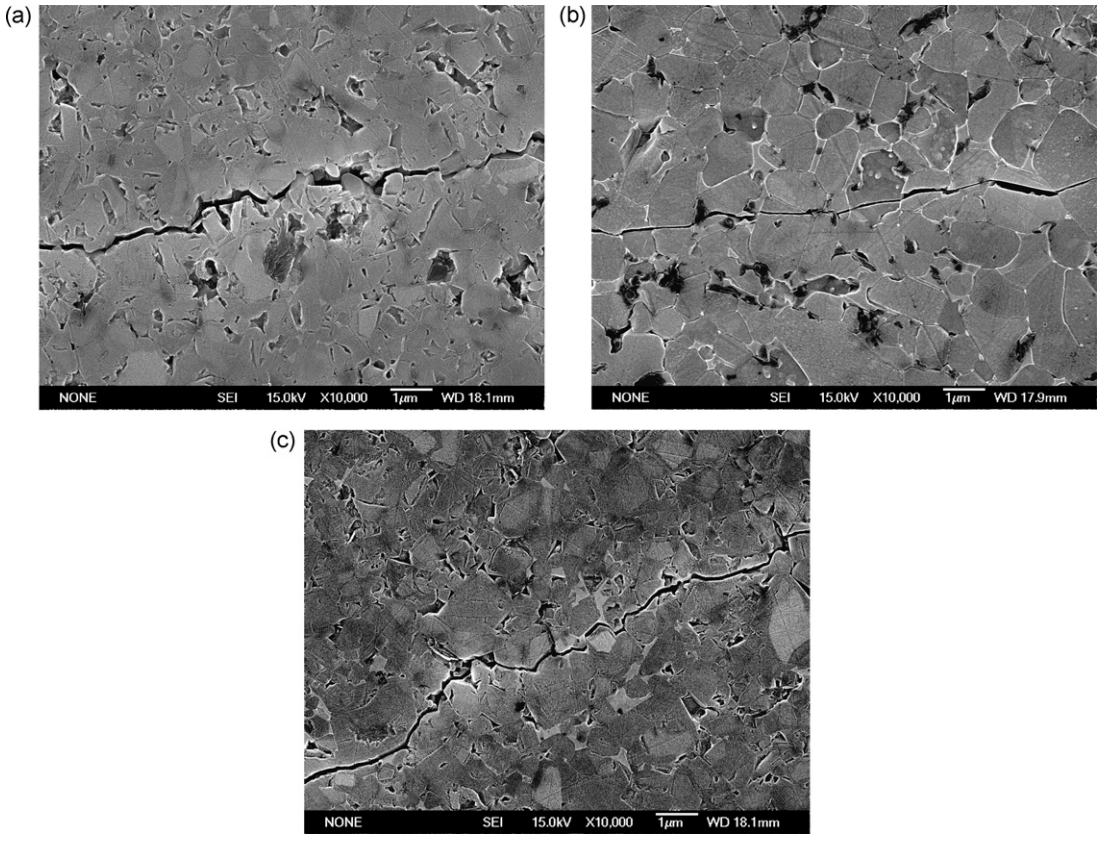

Fig. 5. Microstructure and crack propagation behavior of sintered SiC with 10 wt% additives. (a) Al_3BC_3, SPS anneal, (b) 3Al–B–3C, SPS anneal and (c) Al_3BC_3, SPS.

SiC–$Al_8B_4C_7$ or a mixture of SiC and 10 wt% 8Al–4B–7C (termed SiC–8Al–4B–7C) at 1500 °C in vacuum, sintering shrinkage did not occur up to 1637 °C. Densification of the heat treated powders was completed at 1833–1842 °C during the increase of temperature (Fig. 3(e) and (f)). The sintering shrinkage of the SiC–$Al_8B_4C_7$ was nearly the same with that of the SiC–8Al–4B–7C. The above results indicate that the densification of SiC is not strongly affected by the type of the ternary additives if the chemical composition and amount of the additives are the same. However, the difference of chemical composition (Al_3BC_3 *vs.* $Al_8B_4C_7$) strongly affected the densification behavior of SiC (Fig. 3(a)–(c) *vs.* (d)–(f)). Maitre et al. reported that the densification of SiC was possible at 1950 °C under 100 MPa using SPS when adding boron and carbon additives.[23] In contrast, the sintering of SiC was nearly completed at 1670 °C under 40 MPa pressure by using the $Al_8B_4C_7$ additive. Excess aluminum and boron contained in the $Al_8B_4C_7$ are believed to promote the sintering of SiC compared to the cases using Al_3BC_3 or boron–carbon additives.

Hot-pressed SiC in the presence of the Al–B–C additive has been reported to be densified by a liquid-phase sintering process.[1,5] Zhang et al. reported that molten aluminum and aluminum gas coated SiC grains and reacted with SiO_2 to form viscous grain boundary layer.[5] They observed amorphous grain boundary layers which remained after liquid-phase sintering. In contrast, amorphous layers were not observed in this research (Fig. 4). Yuan et al. reported that the amorphous phase can be fully crystallized during cooling down and the behavior strongly depends on the chemical composition of the Al–B–C.[1] Likewise, an amorphous layer was believed to form and subsequently crystallize during cooling down in the case of the pressureless sintering in this research.

The absence of amorphous layers in between the SiC grains densified using SPS (Fig. 4) may be attributed to the difference of sintering method. The former reports mostly used hot pressing for densification.[1,2,5] In contrast, SPS was applied in the present investigation. During SPS, oxide layers formed on non-oxide ceramic powders were reported to be removed due to the ultra-rapid heating of the powder surface and by the formation of discharge and plasma.[24,25] The formation of a liquid phase might not be strongly enhanced in SiC densified using SPS because SiO_2 might be preferentially removed during heating.

The density of the specimens sintered using the SPS anneal condition (see Table 3) was not strongly affected by the amount of the additive when the additive content was between 3 wt% (termed as SiC–3Al_3BC_3) and 10 wt%. Elongation of the grains did not strongly occur regardless of the additive content up to 10 wt% (Fig. 6) because of the fast heating rate and short holding time at 1900 °C. The spatial diameter of the SiC grains was 2.08 μm, 1.2 μm, 1.55 μm and 0.9 μm when adding 3 wt%, 5 wt% (termed as SiC–5Al_3BC_3), 7.5 wt% and 10 wt% Al_3BC_3, respectively.[17]

The SiC–Al_3BC_3 could be densified by pressureless sintering at and above 1950 °C in Ar. Table 3 summarizes the density of

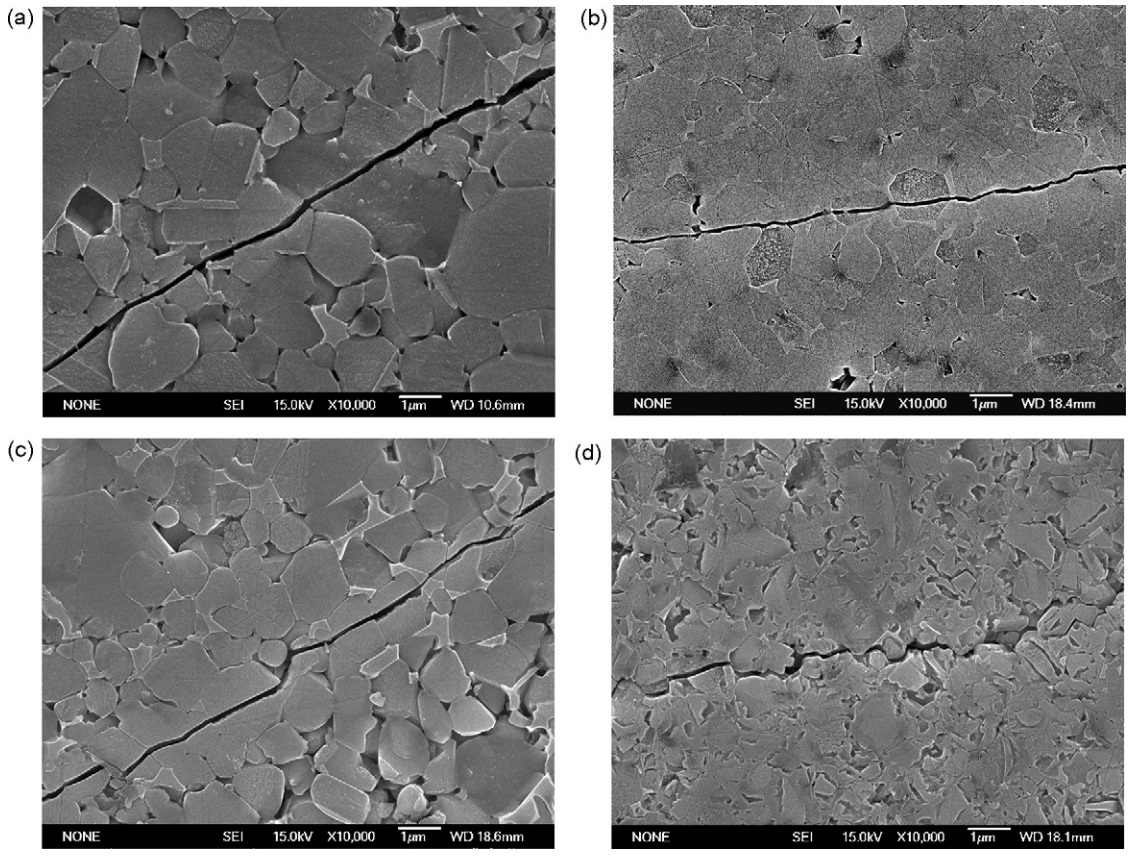

Fig. 6. Microstructure and crack propagation behavior of SiC sintered with the SPS anneal condition. (a) SiC–3Al_3BC_3, (b) SiC–5Al_3BC_3, (c) SiC–7.5Al_3BC_3 and (d) SiC–10Al_3BC_3.

the pressureless sintered SiC–Al_3BC_3. The highest density was attained at 2000 °C and 1950 °C when using 7.5 wt% and 10 wt% Al_3BC_3, respectively. The relative density of the SiC–10Al_3BC_3 was 87.2%, 96.8% and 96.3% after pressureless sintering at 1900 °C, 1950 °C and 2000 °C, respectively.

Fig. 7 shows the microstructure of the pressureless sintered specimens. In contrast to the samples densified by SPS for a short time (3 min), large elongated SiC grains were observed after pressureless sintering for 2 h. The grain size increased (Fig. 7(a)–(c)) and phase transformation from 6H- to 4H-SiC became enhanced with increasing sintering temperature. XRD data clearly indicated the formation of 4H-phase with the consumption of 6H-phase at and above 1950 °C (Fig. 8). SiC grains underwent polytypic transformation during sintering. 6H-SiC grains sintered from α-SiC powder was reported to have isotropic shape.[9] Pure 6H-phase is stable at high temperature and does not transform into other polytypes above 2000 °C.[7] However, transformation into 4H-phase and the elongation of grains were reported to occur in case aluminum dissolved into 6H-SiC grains.[26] EDS analysis informed the dissolution of aluminum in the SiC grains (Fig. 9). EPMA measurement indicated that the amount of dissolved aluminum in SiC grains was 0.6 at.%. The amount of dissolved Al in SiC grains (0.6 at.% ≈ 0.7 wt%) was slightly higher than the solubility limit (0.5 wt% at 2000 °C) reported by Tajima and coworkers.[27] The solubility of B into SiC was reported to be less than 0.1 at.% at 1900 °C.[28] The presence of B in SiC grains could not be detected by EPMA in the present investigation. The measured atomic ratio between Si and C (0.4955:0.5045) indicates that excess carbon exists in the SiC grains. Immobile carbon inclusions at grain boundary were reported to become intragranular inclusions in SiC grains when rapidly migrating grain boundaries moved away from their original positions during grain growth.[29]

3.3. Mechanical properties

The Young's modulus and hardness of Al_3BC_3 and the $Al_8B_4C_7$ were reported to be 153 GPa, 18.2 GPa and 136.6 GPa, 12.1 GPa, respectively,[12,30] indicating that the $Al_8B_4C_7$ is less hard and stiff than Al_3BC_3 presumably because of excess aluminum and carbon. However, the SiC–$Al_8B_4C_7$ had higher Young' modulus and hardness than the SiC–10Al_3BC_3 densified at the same conditions although their density was similar (Table 3). The specimens densified using the SPS anneal condition (see Table 3) have slightly higher density, Young's modulus and hardness than those using the SPS condition presumably due to the decomposition of SiO_2, which is lighter and softer than SiC, during heating at 1500 °C.[31]

Because the Young's modulus and hardness of the ternary aluminum borocarbides are much lower than those of SiC (401 GPa and 33 GPa, respectively),[32] the properties of the SiC–Al_3BC_3 are expected to decrease with increasing the amount of Al_3BC_3. In fact, the Young's modulus value of the SiC–Al_3BC_3 was in

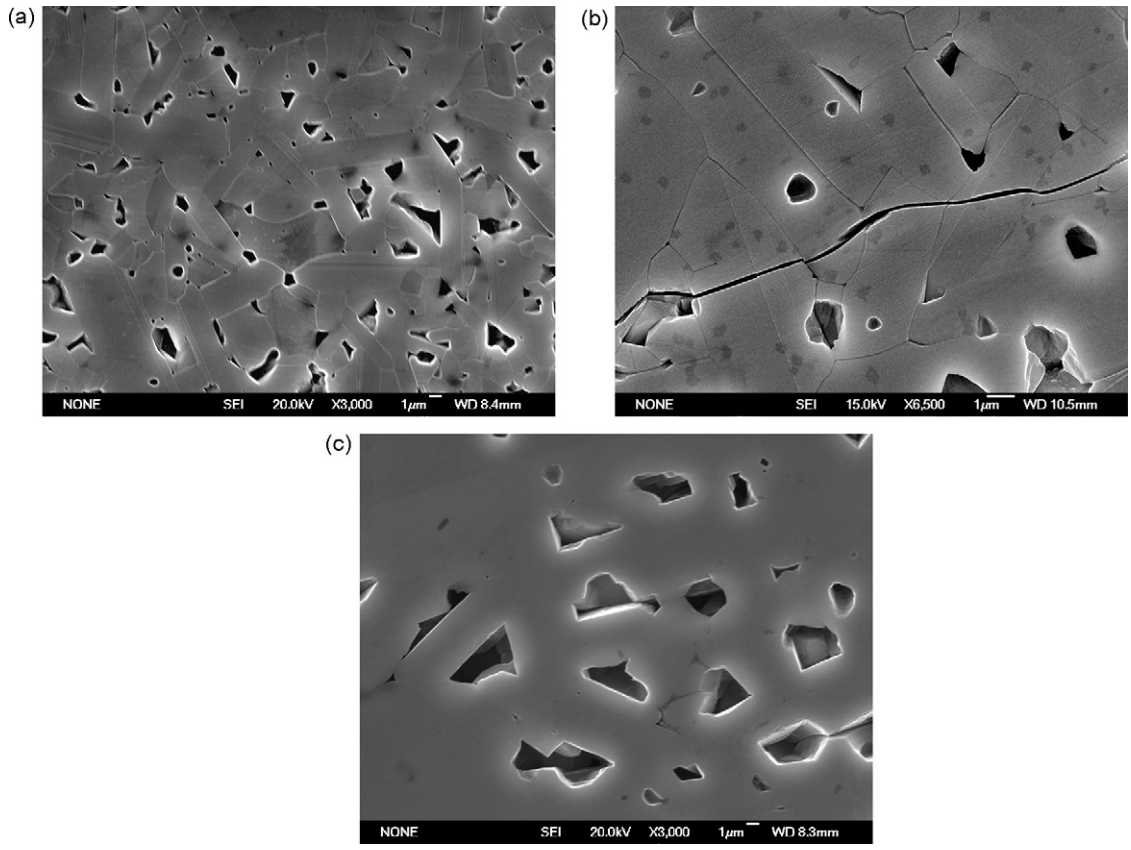

Fig. 7. Microstructure of SiC with 7.5 wt% Al_3BC_3 densified by pressureless sintering for 2 h in Ar at (a) 1950 °C, (b) 2000 °C and (c) 2050 °C.

accordance with the expectation (Table 3). However, the hardness of the specimens did not have clear relationship with the additive content. Hardness and Young's modulus were reported to have proportionality higher than one with the relative density of specimens.[33] Among them, hardness is in many cases more strongly affected by porosity.[34] The difference of porosity is believed to disturb the relationship between hardness and additive content in the SiC–Al_3BC_3.

The Young's modulus and hardness of the pressureless sintered specimens were lower than those obtained by SPS primarily because of the high porosity. The values of the pressureless sintered samples followed the relationship between the mechanical properties and porosity as discussed above.[33]

Yuan et al. reported that SiC sintered with the Al–B–C additives showed inter-granular fracture behavior when having an amorphous grain boundary layer, while crack path became predominantly transgranular in case the layer was fully crystallized.[1] Likewise, transgranular fracture mainly occurred in the specimens which did not have amorphous grain boundary

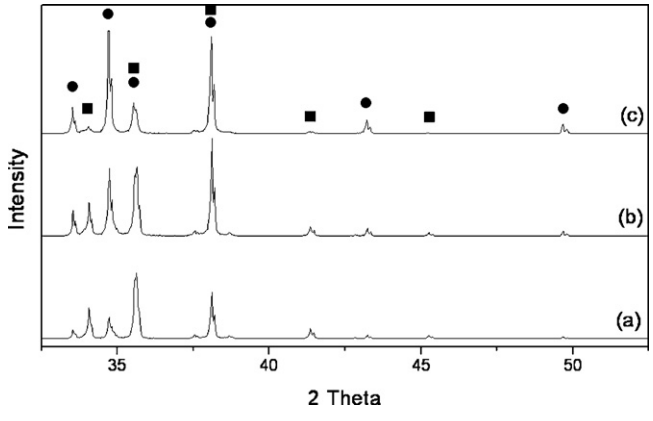

Fig. 8. XRD data of pressureless sintered SiC with 7.5 wt% Al_3BC_3 at (a) 1950 °C, (b) 2000 °C and (c) 2050 °C. (●: 4H-SiC; ■: 6H-SiC).

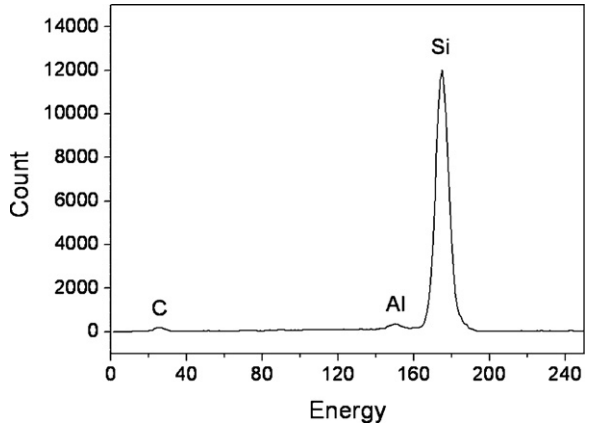

Fig. 9. EDS data of SiC grains after pressureless sintering of SiC + 10 wt% Al_3BC_3 at 1950 °C for 2 h in flowing Ar. EDS was measured at the middle of the grain.

layers in this research. The fracture toughness of the specimens (K_C) was 3.2–4.6 MPa m$^{1/2}$.

While transgranular fracture was the main fracture mechanism of the SiC–3Al–B–3C, inter-granular fracture was also observed in the SiC–10Al_3BC_3 specimens (Fig. 5(a) and (b)). Both the systems have an identical chemical composition and were densified at the same condition. However, the compound additive induced crack deflection as well as suppressed the grain growth of SiC when compared to the conventional Al–B–C additive system. As a result, the fracture toughness of the SiC–10Al_3BC_3 was higher than that of the SiC–3Al–B–3C (K_C: 4.5 MPa m$^{1/2}$ *vs.* 4.0 MPa m$^{1/2}$).[34] The frictional bridging of elongated SiC grains was attributed as the main toughening mechanism of a hot-pressed SiC using the Al–B–C additive.[1] However, crack deflection is believed to be the primary toughening mechanism of the SiC–10Al_3BC_3 densified using SPS because the formation of elongated grains did not distinctly occur due to the fast heating rate and short holding time.

The heating of the powder mixture at 1500 °C before sintering reduced the oxygen content in the powder and increased the onset temperature of sintering shrinkage (Fig. 3). However, the microstructure, fracture behavior and fracture toughness of the SiC–10Al_3BC_3 were not strongly altered by the heating (Fig. 5(a) and (c) and Table 3). In contrast, the treatment increased the fracture toughness of the SiC–3Al–B–3C (4.0 MPa m$^{1/2}$ *vs.* 3.6 MPa m$^{1/2}$) and the SiC–$Al_8B_4C_7$ (4.6 MPa m$^{1/2}$ *vs.* 4.4 MPa m$^{1/2}$). Crack propagation behavior has been reported to be affected by the grain boundary film properties.[1] The results indicated that the reduction of oxygen content by the heating may change the properties of the grain boundary phase, although the difference may not be significant.

The fracture toughness (K_C) of the SiC–3Al_3BC_3 was 3.2 MPa m$^{1/2}$, which value increased with the amount of the additive up to 4.5 MPa m$^{1/2}$. The transition of crack propagation behavior from trans- to inter-granular fracture was observed when the additive content increased from 7.5 wt% to 10 wt% (Fig. 6).

The pressureless sintered specimens had elongated grains, but their fracture toughness values were not higher than those densified by SPS (Table 3). Transgranular fracture was the predominant fracture mechanism of the pressureless sintered SiC (Fig. 7(b)). Accordingly, the beneficial effects originated from elongated grain morphology such as frictional/elastic bridging or crack deflection did not contribute to the toughening of the pressureless sintered SiC.

By using Al_3BC_3 additive instead of the conventional 3Al–B–3C, grain growth of SiC was suppressed and crack deflection behavior was enhanced, which improved the fracture toughness of SiC (4.5 MPa m$^{1/2}$ *vs.* 3.6 MPa m$^{1/2}$). The fracture toughness of SiC was also enhanced by increasing the amounts of Al_3BC_3 (3.2 MPa m$^{1/2}$ *vs.* 4.5 MPa m$^{1/2}$), but at the expense of Young's modulus (415 GPa *vs.* 390 GPa). The difference of chemical composition (Al_3BC_3 *vs.* $Al_8B_4C_7$) had strong effect on the densification of SiC, but the fracture toughness of SiC was not strongly affected by the chemical composition of the additives.

4. Conclusion

The densification of SiC was strongly affected by the chemical composition of the borocarbide additives. Densification of SiC was nearly completed at 1670 °C under 40 MPa pressure when adding the $Al_8B_4C_7$ additive. The new additive systems have benefits compared to the conventional Al–B–C system such as the suppression of grain growth and the easiness of handling in air. In addition, the fracture toughness of SiC was improved by using Al_3BC_3 because of the enhanced crack deflection. The novel aluminum borocarbides are efficient sintering additives of SiC.

References

1. Yuan, R., Kruzic, J. J., Zhang, X. F., De Jonghe, L. C. and Ritchie, R. O., Ambient to high-temperature fracture toughness and cyclic fatigue behavior in Al-containing silicon carbide ceramics. *Acta Mater.*, 2003, **51**(20), 6477–6491.
2. Tokiyama, T., Shinoda, Y., Akatsu, T. and Wakai, F., Enhancement of high-temperature deformation in fine-grained silicon carbide with Al doping. *Mater. Sci. Eng. B*, 2008, **148**(1–3), 261–264.
3. Clough, P. J., Ultra fine powders—their production and characteristic. In *Metallurgical Society Conferences*, *vol. 23*, ed. H. H. Hausner. Gordon and Breach Science Publishers, London, 1964, pp. 9–19.
4. Moberlychan, W. J., Cao, J. J. and De Jonghe, L. C., The roles of amorphous grain boundaries and the β–α transformation in toughening SiC. *Acta Mater.*, 1998, **46**(5), 1625–1635.
5. Zhang, X. F., Sixta, M. E. and De Jonghe, L. C., Grain boundary evolution in hot-pressed ABC–SiC. *J. Am. Ceram. Soc.*, 2000, **83**(11), 2813–2820.
6. Inoue, Z., Tanaka, H. and Inomata, Y., Synthesis and X-ray crystallography of aluminum boron carbide $Al_8B_4C_7$. *J. Mater. Sci.*, 1980, **15**(12), 3036–3040.
7. Tanaka, H., Nishimura, T., Hirosaki, N., Kishi, Y., Matsuo, H. and Ichikawa, Y., Low-temperature sintering of α- and β-SiC powders with AlB_2 additive. *Key Eng. Mater.*, 2006, **317–318**, 23–26.
8. Zhou, Y., Tanaka, H., Otani, S. and Bando, Y., Low temperature sintering of α-SiC with Al_4C_3–B_4C–C additions. *J. Am. Ceram. Soc.*, 1999, **82**(8), 1959–1964.
9. Tanaka, H., Hirosaki, N., Nishimura, T., Shin, D. W. and Park, S. S., Nonequiaxial grain growth and polytype transformation of sintered α-silicon carbide and β-silicon carbide. *J. Am. Ceram. Soc.*, 2003, **86**(12), 2222–2224.
10. Hillebrecht, H. and Meyer, F. D., Synthesis, structure, and vibrational spectra of Al_3BC_3, a carbidecarboborate of aluminum with linear $(C{=}B{=}C)^{5-}$ anions. *Angew. Chem. Int. Ed. Engl.*, 1996, **35**(21), 2499–2500.
11. Rorl, P., *Phase Diagrams of Ternary Metal–Boron–Carbon Systems*. ASM International, Materials Park, OH, 1998, pp. 3–15.
12. Solozhenko, V. L., Solozhenko, E. G. and Lathe, C., Equation of state and thermal stability of Al_3BC. *Solid State Commun.*, 2006, **137**(10), 533–535.
13. Lee, S. H., Kim, H. D., Choi, S. C., Nishimura, T. and Tanaka, H., Densification, mechanical properties and verification of Al-rich aluminum borocarbides. *J. Ceram. Soc. Jpn.*, submitted for publication.
14. Zavaliangos, A., Zhang, J., Krammer, M. and Groza, J. R., Temperature evolution during field activated sintering. *Mater. Sci. Eng. A*, 2004, **379**(1–2), 218–228.
15. Lee, R. C., Aita, C. R. and Tran, N. C., The air-exposed surface of sputter deposited silicon carbide studied by X-ray photoelectron spectroscopy. *J. Vac. Sci. Technol. A*, 1991, **9**(3), 1351–1354.
16. Kim, Y. W., Chun, Y. S., Nishimura, T., Mitomo, M. and Lee, Y. H., High-temperature strength of silicon carbide ceramics sintered with rare-earth oxide and aluminum nitride. *Acta Mater.*, 2007, **55**(2), 727–736.
17. Standard test methods for determining average grain size. *Annual Book of ASTM Standards 2000, ASTM E 112-96*. ASTM, West Conshohocken, PA, 2000.

18. Testing methods for fracture toughness of fine ceramics. *Japanese Industrial Standards, JIS R 1607*. Japanese Standards Association, Tokyo, Japan, 1995.
19. Testing method for hardness of fine ceramics. *Japanese Industrial Standards, JIS R 1610*. Japanese Standards Association, Tokyo, Japan, 2003.
20. Brandt, J. L., Properties of Pure Aluminum. In ed. K. R. van Hohn. In *Aluminum*, *vol. 1*. American Society for Metals, Metals Park, OH, 1967, pp. 1–30.
21. Lide, D. R., ed., *CRC Handbook of Chemistry and Physics*. 86th edition Taylor & Francis group, Boca Raton, FL, 2005. pp. 4-4–4-97.
22. Bibbo, G. S., Benson, P. M. and Pantano, C. G., Effect of carbon monoxide partial pressure on the high-temperature decomposition of Nicalon fiber. *J. Mater. Sci.*, 1991, **26**(18), 5075–5080.
23. Maitre, A., Put, A. V., Laval, J. P., Valette, S. and Trolliard, G., Role of boron on the spark plasma sintering of an α-SiC powder. *J. Eur. Ceram. Soc.*, 2008, **28**(9), 1881–1890.
24. Chaim, R., Densification mechanisms in spark plasma sintering of nanocrystalline ceramics. *Mar. Sci. Eng. A*, 2007, **443**, 25–32.
25. Risbud, S. H. and Groza, J. R., Clean grain boundaries in aluminum nitride ceramics densified without additives by a plasma-activated sintering process. *Philos. Mag. B*, 1994, **69**(3), 525–533.
26. Tanaka, H., Yoshimura, H. N., Otani, S., Zhou, Y. and Toriyama, M., Influence of silica and aluminum contents on sintering of and grain growth in 6H-SiC powders. *J. Am. Ceram. Soc.*, 2000, **83**(1), 226–228.
27. Tana, H., Tajima, Y. and Kingery, W. D., Solid solubility of aluminum and boron in silicon carbide. *Commun. Am. Ceram. Soc.*, 1982, **65**(2), C-27–C-29.
28. Linnarsson, M. K., Zimmermann, U., Leung, J. W., Schöner, A., Janson, M. J., Jagadish, C. and Svensson, B. G., Solubility limits of dopants in 4H-SiC. *Appl. Surf. Sci.*, 2003, **203–204**, 427–432.
29. Braue, W. and Carpenter, R. W., Microscopy of graphite-rich inclusions in sintered α-silicon carbide. *J. Mater. Sci.*, 1990, **25**(6), 2943–2948.
30. Wang, T. and Yamaguchi, A., Some properties of sintered $Al_8B_4C_7$. *J. Mater. Sci. Lett.*, 2000, **19**(12), 1045–1046.
31. Cook, R. F. and Pharr, G. M., Mechanical properties of ceramics. In *Material Science and Technology*, *vol. 11*, ed. R. W. Cahn, P. Haasen and E. J. Kramer. VCH, Weinheim, 1994, pp. 341–360.
32. Kuo, S. Y. and Virkar, A. V., Modulated structures in SiC–AlN ceramics. *Commun. Am. Ceram. Soc.*, 1987, **70**(6), C125–C128.
33. Rice, R. W., Microstructural dependence of mechanical behavior of ceramics. In *Material Science and Technology*, *vol. 11*, ed. R. W. Cahn, P. Haasen and E. J. Kramer. VCH, Weinheim, 1994, pp. 191–381.
34. Faber, K. T. and Evans, A. G., Crack deflection process. 1 Theory. *Acta Mater.*, 1983, **31**(4), 565–576.